

CPW Fed Super-Wideband Antenna for Microwave Imaging Application

Manepalli Sekhar* and Nelaturi Suman

Abstract—A super wideband coplanar waveguide-fed antenna is proposed for Microwave Imaging (MI) applications. The antenna comprising a slotted patch and a defected ground structure (DGS) loaded with a stub has been prototyped on a 1.6 mm thick glass-reinforced FR4 material with an ϵ_r of 4.4. The antenna has a size of $0.12\lambda_0 \times 0.12\lambda_0$ at the lowest operating frequency of 1.21 GHz. The slotted patch coupled well with the stub-loaded DGS in the ground plane and led the proposed antenna to obtain a range of operational bandwidth from 1.21 GHz to 24.66 GHz. Initially, with a rectangular patch, a super wideband antenna with five notch bands is achieved. To eliminate four notch bands and realize the super wideband two rectangular slots are etched in the patch. The last notch band is eliminated by loading the ground with a stub. To make the proposed antenna a compact space-saving one, the patch is fitted in a hexagonal slot etched in the ground. The experimental result reveals a super wideband performance of 181% (1.21 GHz–24.66 GHz) with a consistent radiation pattern and peak gain of 9.4 dB in a compact area of 30 mm².

1. INTRODUCTION

Cancer is becoming one of the main causes of death all around the globe. The early detection of malignant tumors is the best way to treat people effectively, with a high rate of survival. Existing tumor detection technologies use ionic diagnosis procedures which include computer tomography (CT), X-ray mammography, and magnetic resonance imaging (MRI). The resolution of images from these techniques is low and requires interpretation, which may lead to the wrong diagnosis of a tumor. Ionizing radiation is not safe for patients, and in the long run, this may cause cell damage and mutation in DNA by damaging genetic material. Moreover, these detection techniques are not efficient on tumors that are located deep inside the body. To overcome the issues from ionization techniques for tumor detection, a non-ionization detection technique using microwaves is proposed and developed as a microwave imaging (MI) system to replace the current technologies. The MI technology is capable to deliver a high-resolution image irrespective of the tumor location, but the system is complex. The MI system has minimal harm on the patient and can be used in long run for diagnosis [1]. One of the major issues in the MI system is attenuation, as the input power is less than one μW . Microstrip antennas are best suited for the MI system, and their low volume and low power consumption qualities enable the product developers to build compact and transportable devices for the ease of usage. The wide spectrum of frequencies helps develop high-resolution imaging of tumor cells. In recent years patch antennas for super-wideband (SWB)/ultra-wideband (UWB) were published in high volumes [2–31]. Various techniques for designing and enlarging the antenna bandwidth have been documented, including the increase of substrate thickness, using substrates that have very low permittivity, and the insertion of slot/DGS in the patch/ground.

Received 27 December 2022, Accepted 14 February 2023, Scheduled 27 February 2023

* Corresponding author: Manepalli Sekhar (sekhar.ssha@gmail.com).

The authors are with the Department of Electronics and Communication Engineering, Vignans' Foundation for Science, Technology, and Research, Guntur, India.

At microwave frequencies, the interaction of electromagnetic signals with matter depends on the material's dielectric properties, which are the electric permittivity and conductivity. For body tissues, the dielectric properties are related directly to the water content of different biological constituents. In comparison to normal cells, the water content in tumors is high. This can be attributed to the nature of tumor cells that causes them to retain more fluid than normal cells. This extra fluid, which is in the form of bound water, changes the dielectric properties of breast tissues. In MI, tumors are detected using scattered or reflected waves, which arise from the differences in dielectric properties between normal and malignant breast tissues [32].

The use of microwave imaging to detect cancer is achievable due to the difference in the electric properties between healthy and cancerous tissues. Tumors are detected using scattered or reflected waves, which arise from the differences in dielectric properties between normal and malignant tissues. Although the penetration depth in living tissues is considered limited in the microwave frequency range, in MI, the electromagnetic signals need to propagate only for a few centimeters in tissues to provide the information needed for diagnosis [32].

A UWB antenna with a symmetric open slot [5] achieved a resonance of 3.1–13.2 GHz by using a U-shaped feedline. Compared to a meandered ground antenna in [7], the antenna in [5] shows better compactness with a size of 580 mm^2 . An antenna with partial ground with multiple slots and a diamond-shaped patch [9], a slotted ground plane antenna with fowl shaped patch [10], a hybrid U slot antenna [11], and many others are presented in [12–31].

However, the area available on both sides of the substrate in microstrip line-fed antennas is not fully utilized, which results in higher manufacturing costs. co-planar waveguide (CPW)-fed antennas, unlike microstrip line-fed antennas, use most of the patch's space [17]. Both patch and ground lie on the same plane in CPW-fed antennas.

A UWB monopole antenna with CPW feed and open ground stubs was presented in [4]. The antenna's operational band was 3.1–13.2 GHz which is the result of L-shaped stubs. [6] described an antenna with a polygon-shaped patch and CPW feed. The fractal technique is implemented on the patch in this design to increase bandwidth, resulting in an operating range of 7.86 GHz. The patch in [9] by using a fractal geometry has achieved an ultra-wide working band from 2.5 GHz to 10 GHz. [15] described a meandered semicircle-shaped antenna with CPW feed. The developed antenna, which has a total area of $30 \times 35 \text{ mm}^2$, has a percentage bandwidth of 123%. A crown-shaped wideband antenna was constructed on an FR4 substrate [17]. This antenna had a 4.5–13.5 GHz operating band resulting from an expanded U-shaped patch. [19] described a triangle-shaped patch antenna with CPW feed for UWB applications. A top crossloop connects the two ground planes to improve the working band. It does, however, have a 1650 mm^2 overall size. An antenna with coplanar strips and a spiral patch was proposed in [21]. However, because of its big size, it is difficult to install in portable communication systems. [22] proposed an antenna semicircular patch with slots fed with CPW. However, with a surface area of $40 \times 53.3 \text{ mm}^2$, it is unsuitable for microwave imaging applications.

There is a discussion and presentation of a super wideband antenna in [24]. The partial ground plane has been improved by adding five circular sleeves to its top edge and adding five bevelled edges to the antenna patch's vertices. The antenna patch also has a tapered feed. [25] proposes and discusses a Koch fractal patch antenna with SWB characteristics. A step tapered slotted ground plane and two hexagonal Koch fractal radiators with two linear tapered feedlines make up the proposed system, which has a wide operational bandwidth of 1.78 to 30 GHz. [26] presents a unique SWB antenna on a flexible substrate. The Ultralam 3850 substrate, which has dimensions of $60 \times 40 \times 0.1 \text{ mm}^3$, is used to create the circular disc monopole. In [27], a CPW-fed SWB antenna is presented. The adapted antenna consists of an L-shaped and an inverted U-shaped coplanar ground plane, as well as a modified vertical bow-tie-shaped radiator. A compact three-dimensional metamaterial (MTM) loaded portable, inexpensive antenna is described in [28]. The antenna comprises two slotted dipole components with finite arrays of MTM unit cells and a folded parasitic patch that generates directional radiation patterns with 80% fractional bandwidth. [29] presents an MTM loaded three-dimensional stacked wideband antenna array. The antenna is made of three substrate layers, including two air gaps, loaded with metamaterial. The top layer and middle layer have a 1×4 MTM array each, and the bottom layer has a 3×2 MTM array. An MI system with nine antennae and metamaterial loading has been presented in [30]. The suggested antenna is based on a Vivaldi antenna that has been modified. The modified version of Vivaldi antenna

features a single negative metamaterial structure added to improve the far-field antenna properties of antenna which are crucial for MI system. [31] presents a planar UWB antenna for MI systems. The proposed antenna is designed using a partially trapezoidal ground and a slotted semicircular patch. Although most of the antennas mentioned above have reached wide/ultra/super operating bandwidths, several of them have a huge size, making some of them unsuitable for microwave imaging systems.

In this work, a super wideband slotted patch antenna for Microwave Imaging (MI) applications is presented. The needs of MI systems can be met by the ultra-wide impedance bandwidth of 23.45 GHz, ranging from 1.21 GHz to 24.66 GHz with a compact size of $30 \times 30 \times 1.59 \text{ mm}^3$.

2. ANTENNA DESIGN

Figure 1 displays the proposed antenna's geometry. An antenna with dimensions of $30 \text{ mm} \times 30 \text{ mm} \times 1.59 \text{ mm}$ is fabricated on an FR4 substrate after being modeled using HFSS software. Table 1 displays the overall dimensions. The antenna's main radiating component is a rectangle. The top of the patch has two engraved rectangular slots. A hexagonal slot has been etched into the ground plane, and the radiating element is placed inside this hexagonal slot. At the top side of the patch, slotted ground is loaded with a $\lambda/4$ stub. The generation of a super wide bandwidth will be caused by the defective ground loaded with a stub and slotted patches. To obtain a super wide bandwidth, the slots etched in the patch and the stub loaded to the defected ground are helpful. They improve impedance matching and also give orientation to the currents generated in the ground and patch.

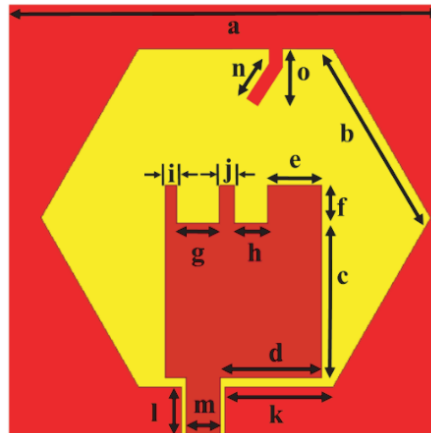


Figure 1. Schematic of Proposed antenna.

Table 1. Optimized parameter of the proposed antenna.

Parameter	Value (mm)	Parameter	Value (mm)	Parameter	Value (mm)
a	30	f	2.5	k	7.5
b	13.5	g	3	l	3.3
c	10.5	h	2.25	m	3
d	7	i	0.75	n	4.5
e	3.75	j	1	o	6.7

Figure 2 shows the evolution of the antenna. The examination of how each antenna element affects the antenna's S parameter is shown in Figure 3. Antenna 1 is a rectangular strip that is CPW-fed and placed in the ground with a hexagonal slot. This antenna's impedance matching is subpar, and a wideband of resonance covering the range of 9.36 GHz to 14.60 GHz is noted for it. Antenna 2 is

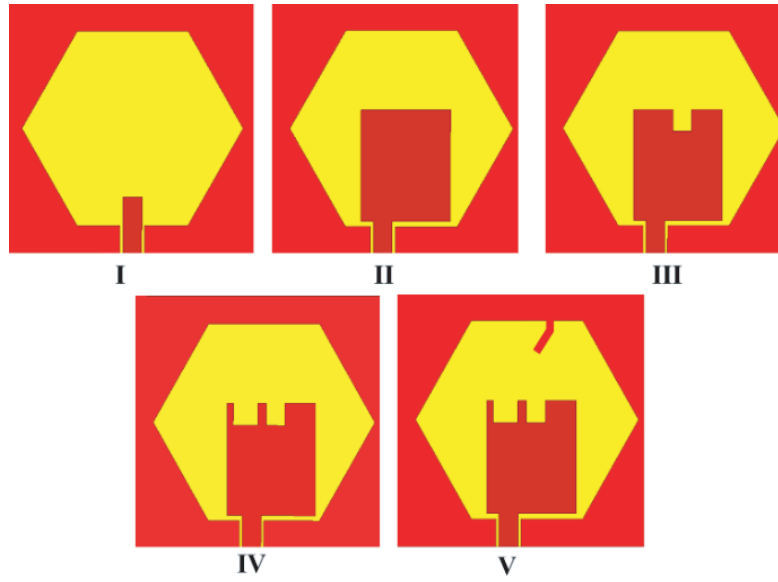


Figure 2. Different stages of proposed antenna evolution.

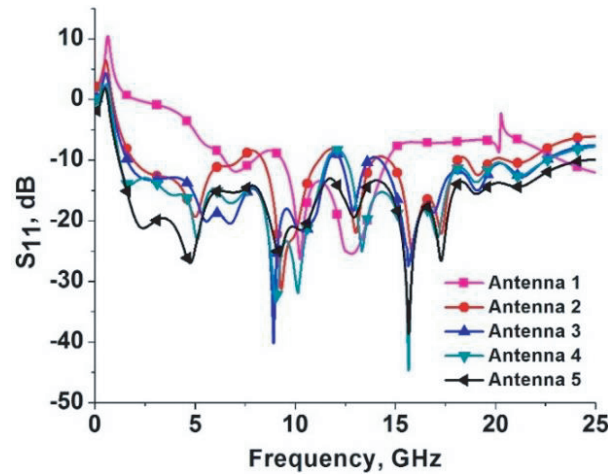


Figure 3. Simulations of S_{11} at different stages.

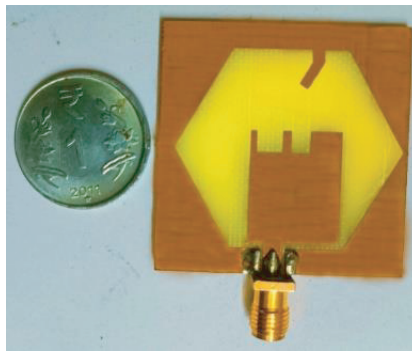
a rectangular patch antenna that is CPW fed and placed in the ground with a hexagonal slot. The position of the hexagonal slot is shifted to the right by 1 mm, and the location of the feed line is shifted to the left by 3 mm. As a result, antenna 2's impedance matching is improved, and this antenna exhibits a super wide resonance with five notch bands with center frequencies of 7.93 GHz, 11.83 GHz, 14.36 GHz, 18.37 GHz, and 20.13 GHz. In antenna 3 the first rectangular slot is etched on the topside of the rectangular patch. With this, the impedance matching of the antenna at 7.93 GHz, 18.37 GHz, and 20.13 GHz improved, and the notch bands at these frequencies are eliminated leaving only two notch bands at 11.83 GHz and 14.36 GHz. In antenna 4 one more rectangular slot is etched in the patch. It improved impedance matching at 14 GHz, and the notch band at 14.36 GHz is eliminated. The slotted ground plane is loaded with a $\lambda/4$ stub which protrudes into the hexagonal slot as shown in antenna 5. This stub improved the antenna's impedance matching at 11.83 GHz and eliminated the notch at 11.83 GHz which resulted in the super wideband performance of 23.45 GHz (181%) ranging from 1.21 GHz to 24.66 GHz.

3. RESULTS AND DISCUSSION

The antenna prototype is made, and the setup for experimental verification is shown in Figure 4. Figure 4(a) shows the antenna prototype and S_{11} measurement using keysight series network analyzer E5063A (shown in Figure 4(b)). The gain and radiation pattern measuring setup for the antenna is shown in Figure 4(c). The measured and simulated results are compared to each other and are consistent.

HFSS software is used to optimize and analyze the proposed antenna. Figure 5 shows the antenna's simulated and measured impedance bandwidths, with the measured bandwidth showing good agreement.

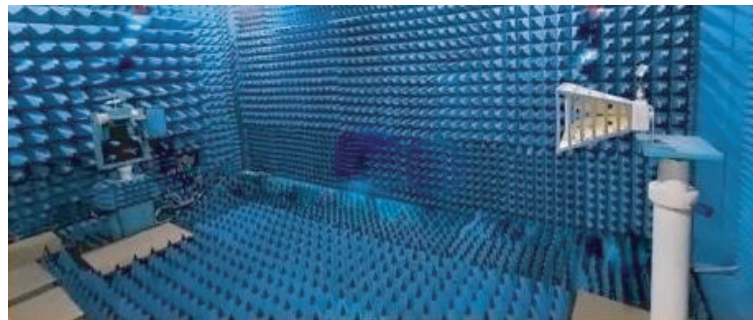
To help understand the operation of the proposed antenna, various antenna design parameters were altered while various configurations of the antenna are analyzed. Figures 6 and 7 show the comparison



(a)



(b)



(c)

Figure 4. Antenna prototype and measurement setup. (a) Fabricated antenna. (b) Antenna S_{11} measurement setup. (c) Antenna measurement setup in an anechoic chamber.

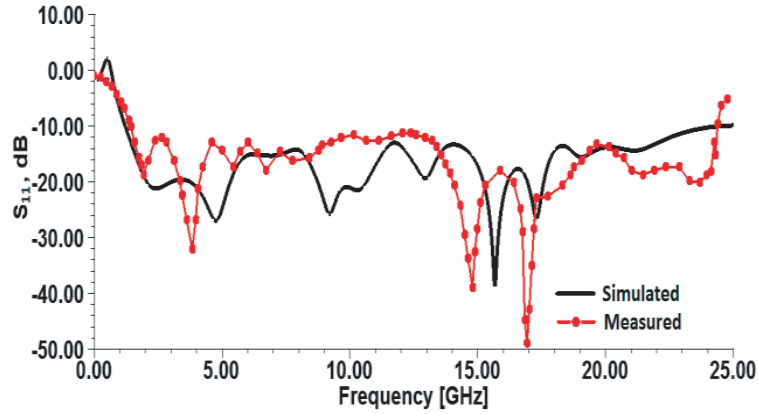


Figure 5. Simulated and measured S parameters.

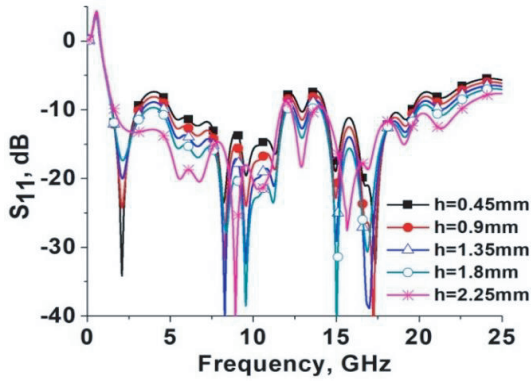


Figure 6. Effect of first rectangular slot width on S_{11} .

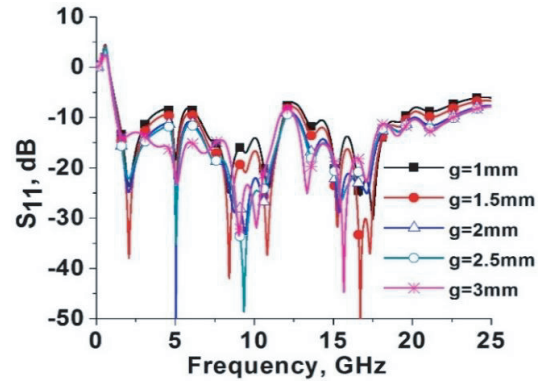


Figure 7. Effect of second rectangular slot width on S_{11} .

of S -parameter plots of various antenna configurations. Figure 6 shows how changing the width of the first rectangular slot in the patch, and Figure 7 shows how changing the width of the second rectangular slot affects the antenna S_{11} .

With the addition of slots in the patch, it is seen that the notch bands at 7.93 GHz, 18.37 GHz, and 20.13 GHz got eliminated. The slots created new radiating edges in the patch, which increased the corresponding currents in the patch and changed the antenna's impedance. The notch bands were

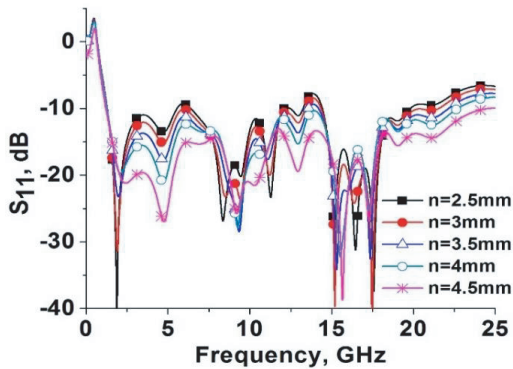


Figure 8. Effect of $\lambda/4$ stub on S_{11} .

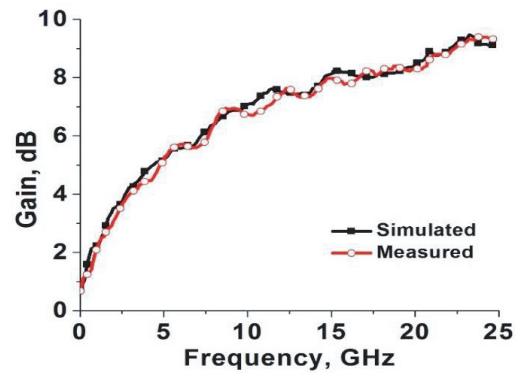
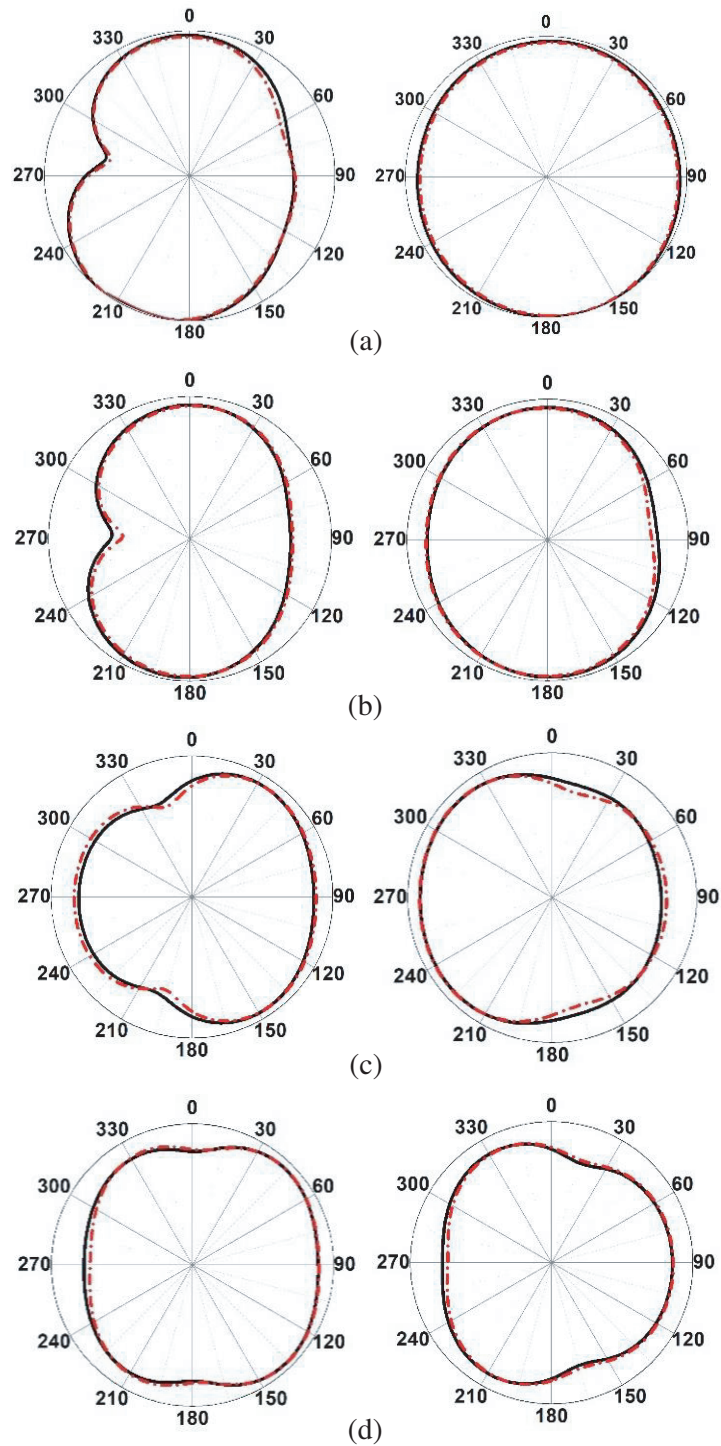


Figure 9. Simulated and measured gain.

reduced by tuning the slots' size while creating new operating frequencies. As a result, by reducing the notch bands, the slots etched into the patch increased bandwidth. The effect on antenna S_{11} due to $\lambda/4$ stub loaded in the ground is shown in Figure 8. S_{11} of the antenna is analyzed by varying the length of the stub. The bandwidth and impedance matching of the antenna vary with the increase of the stub length. With the introduction of the stub with $\lambda/4$ length of the notch band frequency, the impedance of the antenna is altered to resonate the antenna at 11.83 GHz.

Figure 9 shows the antenna's simulated and measured gains. It has a peak gain of 9.4dB, a



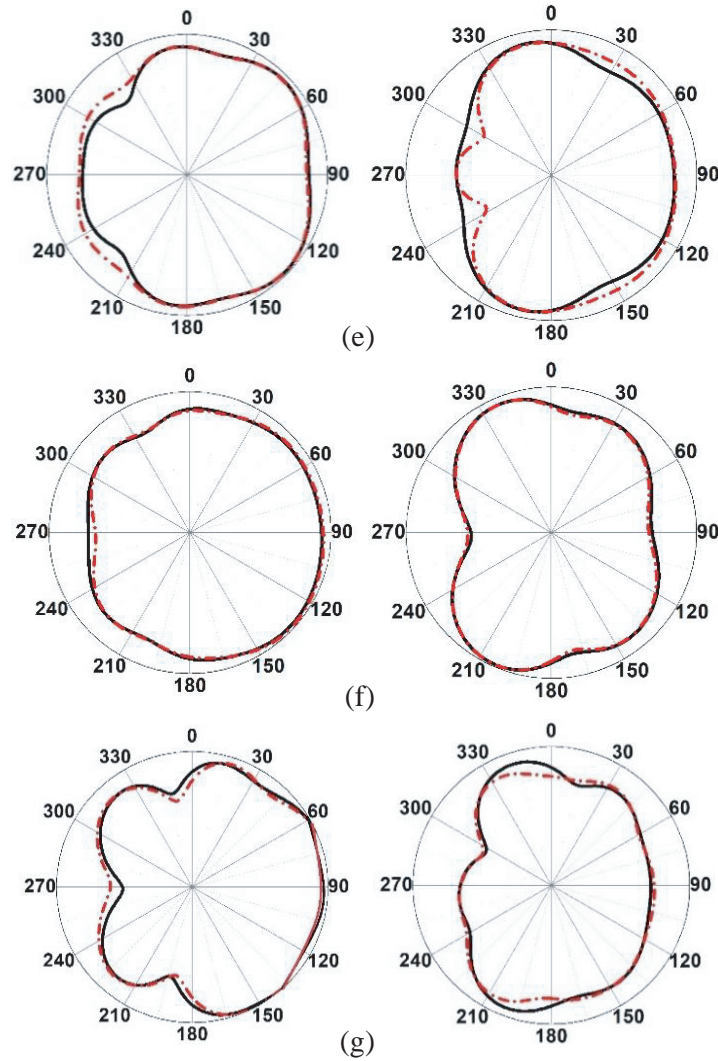


Figure 10. Radiation patterns (*E*-plane and *H*-plane). (a) 3 GHz. (b) 6 GHz. (c) 9 GHz. (d) 12 GHz. (e) 15 GHz. (f) 18 GHz. (g) 22 GHz.

consistent omnidirectional radiation pattern, and a small footprint of 30 mm^2 . Due to the antenna's small size, the gain at lower operating frequencies is lower than at higher working frequencies.

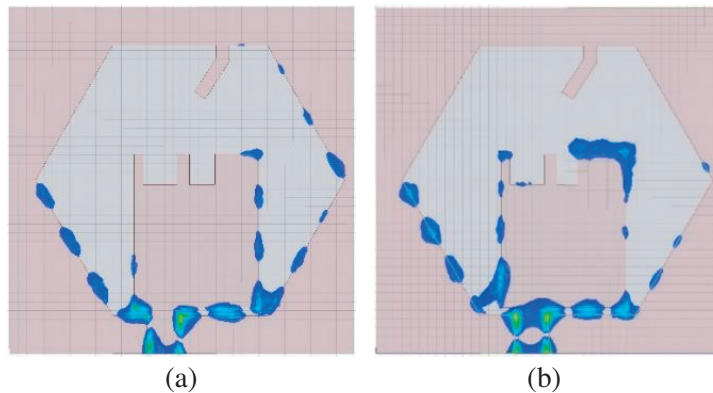
Figure 10 displays the antenna's 2D radiation patterns at various intermediate frequencies. At all frequencies, the *E* and *H* planes both display omnidirectional patterns. The results support the antenna's omnidirectional capabilities, which are appropriate for MI applications.

Figure 11 depicts the current distributions at 2.5 GHz, 8 GHz, 12 GHz, 14 GHz, 18 GHz, and 20 GHz. The contribution of the patch and ground plane for radiation at all frequencies can be observed from the plots. In the plot of Figure 11(a), we can observe that majority of the current fields are excited at the edges of the patch and ground plane at 2.5 GHz. We have etched slot 1 to eliminate the notch bands at 7.93 GHz, 18.37 GHz, and 20.13 GHz, and the same can be observed from plots of Figure 11(b), (e), and (f) where current fields have extended to slot 1 region at the frequencies of 8 GHz, 18 GHz, and 20 GHz. Further, we have etched slot 2 to eliminate the notch band at 14.36 GHz, and we can observe from plot of Figure 11(d) that the current fields have extended to the slot 2 regions at 14 GHz. Finally, we have loaded the $\lambda/4$ stub in the ground plane to eliminate the notch band at 11.83 GHz, and we can observe from plot of Figure 11(c) that the current fields are extended to the stub loaded in the ground at 12 GHz. From this we can observe the significance of the slots and stubs in the generation of the super wideband performance of the antenna.

Table 2 compares the proposed antenna with reported ultra/super wideband antennas. The proposed antenna performs better in terms of gain, impedance bandwidth, and antenna profile.

Table 2. Comparison of the presented antenna with other ultra/super wideband antennas reported.

Ref.	Size (λ_0^2)	Operating band (GHz)	Fractional bandwidth (%)	Peak Gain (dB)
2	0.25×0.30	1.94–15.4	155	6
3	0.23×0.19	3.55–12.16	110	4.52
4	0.21×0.30	3.15–10.55	108	5.7
5	0.25×0.25	3.0–10.85	113	3
6	0.31×0.23	3.1–17.1	139	4.2
7	0.22×0.27	2.8–11.5	122	5.8
8	0.23×0.23	2.5–10	120	3.35
9	0.25×0.36	3.1–12.3	119	6.8
10	0.3×0.3	3.0–20	148	6
11	0.31×0.31	3.04–11	113	5.1
12	0.34×0.30	2.96–12	121	3.82
13	0.34×0.40	3.42–11.7	110	6
14	0.31×0.36	3.1–13.1	123	5
15	0.23×0.33	2.18–20	161	4.38
16	0.63×0.54	4.5–13.5	100	6.08
24	0.4×0.4	3.37–27.71	157	7.8
25	0.14×0.21	1.78–30	178	6.6
26	0.34×0.23	1.96–67	189	10.4
27	0.25×0.20	3.03–17.39	1471	4.56
28	0.45×0.19	1.95–4.5	80	6
29	0.22×0.18	1.37–3.16	79	6.67
30	0.26×0.30	2.0–10.45	136	7.9
31	0.3×0.31	2.3–11.0	130	5.8
This Work	0.12×0.12	1.21–24.66	181	9.4



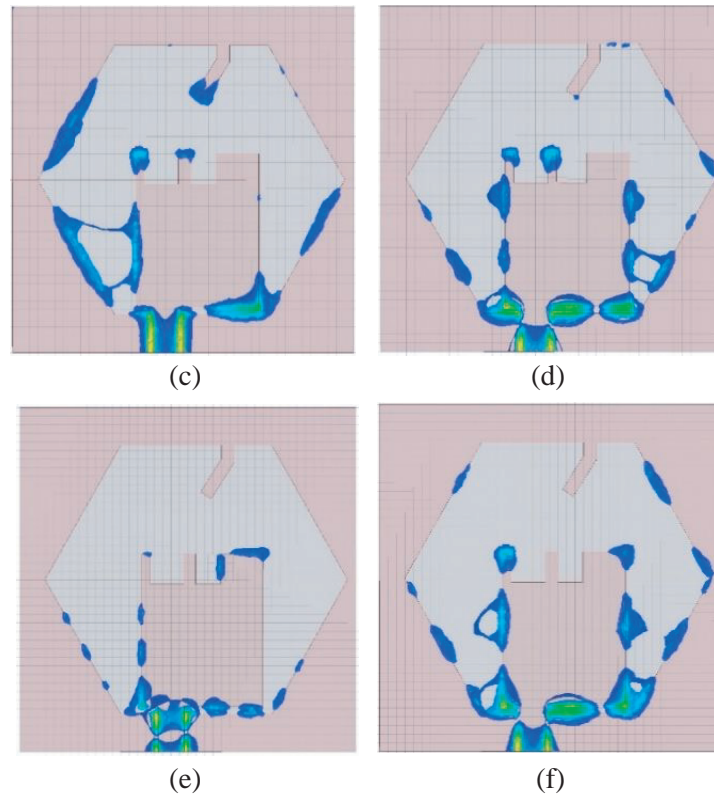


Figure 11. Current distributions at different frequencies. (a) 2.5 GHz. (b) 8 GHz. (c) 12 GHz. (d) 14 GHz. (e) 18 GHz. (f) 20 GHz.

4. CONCLUSION

A compact super wideband CPW-fed antenna for Microwave Imaging (MI) applications is presented. Initially, with a rectangular patch, a super wideband antenna with five notch bands is achieved. Two rectangular slots are etched in the patch to eliminate four notch bands and realize the super wideband. The last notch band is eliminated by loading the ground with a $\lambda/4$ stub. To make the proposed antenna a compact space-saving one, the entire model is fitted in a hexagonal slot in the antenna ground. The measured result reveals a good super wideband performance of 181% (1.21 GHz–24.66 GHz). It has a peak gain of 9.4 dB, a consistent omnidirectional radiation pattern, and a compact size of 30 mm^2 . The antenna composed of a slotted patch and a defective ground structure (DGS) has been prototyped on a 1.6 mm thick FR4 material. The antenna has a size of $0.12\lambda_0 \times 0.12\lambda_0$ at the lowest operating frequency of 1.21 GHz. The slotted patch coupled well with the DGS in the ground plane leading the proposed antenna to obtain a range of operational bandwidth from 1.21 GHz to 24.66 GHz.

REFERENCES

1. Jalilvand, M., X. Li, L. Zwirello, and T. Zwick, "Ultrawideband compact near-field imaging system for breast cancer detection," *IET Microwaves, Antennas & Propagation*, Vol. 9, No. 10, 1009–1014, 2015.
2. Bala, S., P. Soni Reddy, S. Sarkar, and P. P. Sarkar, "Small size wideband monopole antenna with five notch bands for different wireless applications," *Radioengineering*, Vol. 31, No. 1, 23–31, 2022.
3. Rizvi, S. N. R., W. A. Awan, and N. Hussain, "Design and characterization of miniaturized printed antenna for UWB communication systems," *Journal of Electrical Engineering and Technology*, Vol. 16, No. 2, 1003–1010, 2021.

4. Tan, M. T., J. Q. Li, and Z. Y. Jiang, "A miniaturized ultra-wideband planar monopole antenna with L-shaped ground plane stubs," *Int. J. RF Microw. Comput. Aided Eng.*, Vol. 29, No. 11, 1–7, 2019.
5. Zhang, S., Y. Zhong, Y. Zhou, Y. Guo, and C. Ji, "Design of a symmetric open slot antenna for UWB applications," *IEICE Electron Expr.*, Vol. 16, No. 20, 2019.
6. Fallahi, H. and Z. Atlasbaf, "Bandwidth enhancement of a CPW-fed monopole antenna with small fractal elements," *AEU — Int. J. Electron. Commun.*, Vol. 69, No. 2, 590–595, 2015.
7. Sahoo, S., L. P. Mishra, M. N. Mohanty, and R. K. Mishra, "Design of compact UWB monopole planar antenna with modified partial ground plane," *Microw. Opt. Technol. Lett.*, Vol. 60, No. 3, 578–583, 2018.
8. Hossain, A., M. T. Islam, A. F. Almutairi, M. S. J. Singh, K. Mat, and M. Samsuzzaman, "An octagonal ring-shaped parasitic resonator based compact ultrawideband antenna for microwave imaging applications," *Sensors*, Vol. 20, No. 5, 1354, 2020.
9. Dwivedi, R. P. and U. K. Kommuri, "Compact high gain UWB antenna using fractal geometry and UWB-AMC," *Microw. Opt. Technol. Lett.*, Vol. 61, No. 3, 787–793, 2019.
10. Hossain, M. J., M. R. I. Faruque, M. M. Islam, M. T. Islam, and M. A. Rahman, "Bird face microstrip printed monopole antenna design for ultra wide band applications," *Frequenz*, Vol. 70, Nos. 11–12, 473–478, 2016.
11. Elhabchi, M., M. N. Srifi, and R. Touahni, "A novel modified U-shaped microstrip antenna for Super Wide Band (SWB) applications," *Analog Integr. Circuits Signal Process.*, Vol. 102, No. 3, 571–578, 2020.
12. Mahmud, M. Z., M. T. Islam, and M. Samsuzzaman, "A high performance UWB antenna design for microwave imaging system," *Microw. Opt. Technol. Lett.*, Vol. 58, No. 8, 1824–1831, 2016.
13. Midya, M., S. Bhattacharjee, and M. Mitra, "Circularly polarized planar monopole antenna for ultrawideband applications," *Int. J. RF Microw. Comput.-Aided Eng.*, Vol. 29, No. 11, 1–9, 2019.
14. Awad, N. M. and M. K. Abdelazeez, "Multi-slot microstrip antenna for ultra-wide band applications," *J. King Saud Univ. Eng. Sci.*, Vol. 30, No. 1, 38–45, 2018.
15. Kundu, S. and S. K. Jana, "A compact umbrella shaped UWB antenna for ground-coupling GPR applications," *Microw. Opt. Technol. Lett.*, Vol. 60, No. 1, 51–146, 2018.
16. Dorostkar, M. A., M. T. Islam, and R. Azim, "Design of a novel super wide band circular-hexagonal fractal antenna," *Progress In Electromagnetics Research*, Vol. 139, 229–245, 2013.
17. Sharma, A., P. Khanna, K. Shinghal, and A. Kumar, "Design of CPW fed antenna with defected substrate for wideband applications," *J. Electr. Comput. Eng.*, Vol. 2016, 1–10, 2016.
18. Azim, R., M. T. Islam, and N. Misran, "Microstrip line-fed printed planar monopole antenna for UWB applications," *Arabian J. Sci. Eng.*, Vol. 38, No. 9, 2415–2422, 2013.
19. Zhang, D. and Y. Rahmat-Samii, "Top-cross-loop improving the performance of the UWB planar monopole antennas," *Microw. Opt. Technol. Lett.*, Vol. 59, No. 10, 2432–2440, 2017.
20. Kumar, R., R. Sinha, A. Choubey, and S. K. Mahto, "An ultrawide band monopole antenna using hexagonal-square shaped fractal geometry," *Journal of Electromagnetic Waves and Applications*, Vol. 35, No. 2, 233–244, 2021.
21. Omar, A. A., O. A. Safia, and M. Nedil, "UWB coplanar waveguide-fed coplanar strips rectangular spiral antenna," *Int. J. RF Microw. Comput. Aided Eng.*, Vol. 27, No. 7, 1–6, 2017.
22. Telsang, T. M. and A. B. Kakade, "Ultra-wideband slotted semi-circular patch antenna," *Microw. Opt. Technol. Lett.*, Vol. 56, No. 2, 362–369, 2014.
23. Samsuzzaman, M. and M. T. Islam, "A semicircular shaped super wideband patch antenna with high bandwidth dimension ratio," *Microw. Opt. Technol. Lett.*, Vol. 57, No. 2, 445–452, 2015.
24. Faouri, Y., S. Ahmad, S. Naseer, K. Alhammami, N. Awad, A. Ghaffar, and M. I. Hussein, "Compact SWB frequency diversity hexagonal shaped monopole antenna with switchable rejection band," *IEEE Access*, Vol. 10, 42321–42333, 2022.
25. Chaudhary, A. K. and M. Manohar, "Modified SWB hexagonal fractal spatial diversity antenna with high isolation using meander line approach," *IEEE Access*, Vol. 10, 10238–10250, 2022.

26. Dey, S., Md. S. Arefin, and N. C. Karmakar, "Design and experimental analysis of novel compact and flexible SWB antenna for 5G," *IEEE Access*, Vol. 9, 46698–46708, 2021.
27. Azim, R., M. T. Islam, H. Arshad, Md. M. Alam, N. Sobahi, and A. I. Khan, "CPW-fed super-wideband antenna with modified vertical bow-tie-shaped patch for WSNs," *IEEE Access*, Vol. 9, 5343–5353, 2021.
28. Islam, M. S., M. T. Islam, and A. F. Almutairi, "A portable non-invasive microwave based head imaging system using compact metamaterial loaded 3D unidirectional antenna for stroke detection," *Scientific Reports*, Vol. 12, 8895, 2022.
29. Hossain, A., M. T. Islam, G. K. Beng, S. B. A. Kashem, M. S. Soliman, N. Misran, and M. E. H. Chowdhury, "Microwave brain imaging system to detect brain tumor using metamaterial loaded stacked antenna array," *Scientific Reports*, Vol. 12, 16478, 2022.
30. Islam, M. T., M. T. Islam, Md Samsuzzaman, H. Arshad, and H. Rmili, "MTM loaded nine high gain Vivaldi antennas array for microwave breast imaging application," *IEEE Access*, Vol. 8, 227678–227689, 2020.
31. Hossain, A., M. T. Islam, Md. T. Islam, M. E. H. Chowdhury, H. Rmili, and Md. Samsuzzaman, "A planar ultrawideband patch antenna array for microwave breast tumor detection," *Materials*, Vol. 13, 4918, 2020.
32. AlSawaftah, N., S. El-Abed, S. Dhou, and A. Zakaria, "Microwave imaging for early breast cancer detection: Current state, challenges, and future directions," *J. Imaging*, Vol. 8, 123, 2022.